Molecular Dynamics Simulations of the Solution−Air Interface of Aqueous Sodium Nitrate

Jennie L. Thomas,[†] Martina Roeselová,*[,‡] Liem X. Dang,[§] and Douglas J. Tobias*[,†]

Environmental Molecular Science Institute and Department of Chemistry, University of California, Irvine, California 92697, Center for Biomolecules and Complex Molecular Systems, Institute of Organic Chemistry and Biochemistry, Academy of Sciences of the Czech Republic, Flemingovo nam. 2, 16610 Prague 6, Czech Republic, Chemical Sciences Division, Pacific Northwest National Laboratory, Richland, Washington 99352

Received: December 6, 2006; In Final Form: February 12, 2007

Molecular dynamics simulations have been used to investigate the behavior of aqueous sodium nitrate in interfacial environments. Polarizable potentials for the water molecules and the nitrate ion in solution were employed. Calculated surface tension data at several concentrations are in good agreement with measured surface tension data. The surface potential of $NaNO_3$ solutions at two concentrations also compare favorably with experimental measurements. Density profiles suggest that NO_3^- resides primarily below the surface of the solutions over a wide range of concentrations. When the nitrate anions approach the surface of the solution, they are significantly undercoordinated compared to in the bulk, and this may be important for reactions where solvent cage effects play a role such as photochemical processes. Surface water orientation is perturbed by the presence of nitrate ions, and this has implications for experimental studies that probe interfacial water orientation. Nitrate ions near the surface also have a preferred orientation that places the oxygen atoms in the plane of the interface.

Introduction

Renewed interest in ions at aqueous interfaces was initiated by experiments in which measured $Cl_{2(g)}$ and $Br_{2(g)}$ uptake over NaI and NaBr solutions could not be explained with a simple bulk-phase reaction mechanism.[1] This observation, combined with theoretical calculations on negative ions in water clusters, provided initial evidence for interfacial solvation of polarizable ions.[2,3] Subsequent work on interface reactions between surface halide ions and atmospheric oxidants[4−7] has fueled further theoretical studies on aqueous interfaces.[8−18] In addition, second harmonic generation (SHG)[19−24] and vibrational sum frequency generation (VSFG)[25−27] studies on ions at aqueous interfaces have advanced our understanding of these systems. Surface propensity of ions is also closely tied to measured interfacial properties such as surface potential and surface tension. Work to resolve the molecular level theoretical[28,29] and spectroscopic[23,25,26] understanding of aqueous interfaces with macroscopic thermodynamic properties[30−32] is ongoing.

The importance of nitrate in the atmosphere has been highlighted by the recent focus of both atmospheric and physical chemistry on research related to this topic.[11,18,25,33−49] Nitrate is incorporated into sea salt particles in the atmosphere via atmospheric aging processes, involving oxides of nitrogen such as HNO_3, NO_2, N_2O_5, and $ClONO_2$, in which chloride ions are displaced by nitrate.[50−56] Aqueous nitrate ions are abundant in the atmosphere and are involved in a variety of atmospheric reactions.[57] In this article, we investigate the behavior of aqueous $NaNO_3$ in interfacial environments using classical molecular dynamics (MD) simulations.

VSFG studies have suggested that $0.2x$ $NaNO_3$ (x = mole fraction) modifies the first layer of surface water molecules compared to neat water.[25] However, the detailed structure (e.g., location and orientational distribution) of interfacial water molecules and nitrate ions is not known. Comparing VSFG spectra and MD simulations[29,58−63] has provided insight into the details of interfacial water structure in neat water, sodium halide solutions,[28] and aqueous acids and bases,[27] but this has not yet been done for aqueous interfaces containing nitrate ions.

Computational studies on NO_3^- at the aqueous interface have produced conflicting results concerning the propensity for the nitrate anion for the air−water interface.[11,18,38] In this study, we set out to answer the question: is NO_3^- present at the surface of aqueous $NaNO_3$ solutions? Because of these conflicting results, we first validate our simulation model by comparing calculations of surface tension data for aqueous $NaNO_3$ at three concentrations and surface potentials at two concentrations to experimental data. After model validation, we repeat the calculations of Salvador et al.[38] and report on the behavior of one $NaNO_3$ in a water slab, also referred to as nitrate at infinite dilution (in our case, this corresponds to approximately 0.05 M $NaNO_3$). Then we extend our study to NO_3^- at finite concentrations of 1.5 and 6.8 M. On the basis of these simulations, we predict that nitrate resides primarily in the bulk, and there is only a small amount of NO_3^- at the air−water interface. We observed that water coordination around nitrate ions near the interface differs from the water coordination around bulk ions, and this suggests that nitrate ions could experience unique interfacial chemistry. Surface water orientation is also disrupted by the presence of nitrate ions. Finally, the orientation of nitrate ions near the liquid−vapor interface versus the bulk is presented in order to provide a basis for understanding future spectroscopic studies that probe nitrate ions directly.

* To whom correspondence should be addressed. E-mail: martina.roeselova@uochb.cas.cz (M.R.); dtobias@uci.edu (D.J.T.).

[†] Environmental Molecular Science Institute and Department of Chemistry, University of California, Irvine.

[‡] Center for Biomolecules and Complex Molecular Systems, Institute of Organic Chemistry and Biochemistry.

[§] Chemical Sciences Division, Pacific Northwest National Laboratory.

10.1021/jp0683972 CCC: $37.00
Published on Web 04/03/2007

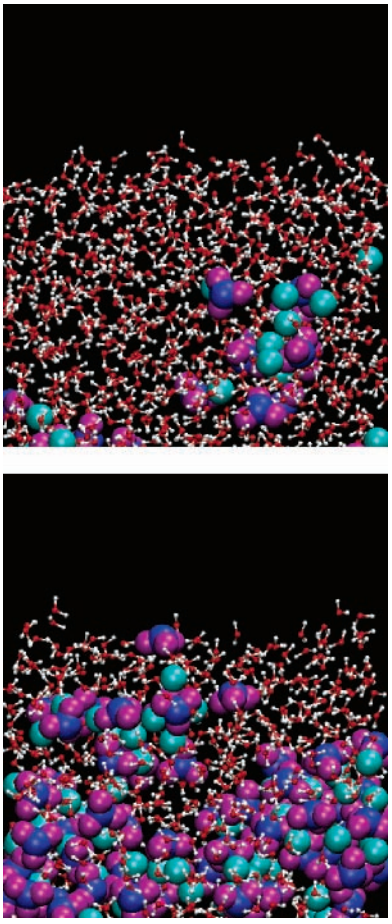

Figure 1. Snapshots from simulations of the liquid/vapor interface of 1.5 and 6.8 M $NaNO_{3(aq)}$. N = blue, O_N = purple, Na = teal, O_W = red, H_W = white.

Computational Methods

Simulations of aqueous $NaNO_3$ were completed using classical molecular dynamics of $NaNO_3$ in a box of 864 water molecules with periodic boundary conditions in three dimensions.[64] To simulate the liquid−vapor interface, a slab geometry[65,66] was employed as in previous studies (see for example refs 14, 27, 38). The size of the unit cell was set to 30 Å × 30 Å × 100 Å, with the elongated box dimension along the *z* axis normal to the two liquid−vapor interfaces. Snapshots of one interface from simulations of 1.5 and 6.8 M $NaNO_3$ solutions are shown in Figure 1. The simulations were carried out at constant volume and a constant temperature of 298 K.

All simulations were completed using the Amber 8 suite of programs.[67] Long-range electrostatic interactions were calculated using the particle mesh Ewald method[68,69] with a real space cutoff of 12 Å. Water molecules were modeled using the polarizable POL3 water model,[70] and the internal degrees of freedom of the water molecules were constrained using the SHAKE algorithm.[71] Each simulation consisted of at least 500 ps equilibration, followed by 2−4 ns of data collection, using a time step of 1 fs. This simulation length was sufficient to produce density profiles that differ in the nitrate peak height by less than 15% on opposite sides of the slab. For the surface potential calculations, a time step of 2 fs was used. To avoid the well-known polarization catastrophe[72] due to the large electric field in solutions with high ionic strengths, the induced dipoles were calculated using a method developed previously for calculations on sodium thiocyanate,[21] with the induced dipole scaling chosen to preserve the properties of neat water.[21]

TABLE 1: Simulation Parameters for NO_3^- Given in the Amber Convention[a]

	atom	*q* (e)	α (Å^3)	R_m (Å)	ϵ (kcal/mol)
		Prior Work			
Salvador et al.[38]	N (nitrate)	+0.950	0.000	2.180	0.200
	O (nitrate)	−0.650	1.300	1.760	0.155
Minofar et al.[18]	N (nitrate)	+0.950	0.000	1.880	0.170
	O (nitrate)	−0.650	1.200	1.800	0.160
		This Study			
parameter set A[38]	N (nitrate)	+0.950	0.000	2.180	0.200
	O (nitrate)	−0.650	1.490	1.760	0.155
parameter set B[18]	N (nitrate)	+0.950	0.000	1.880	0.170
	O (nitrate)	−0.650	1.490	1.800	0.160

[a] In the present study, calculations were completed using both sets of Lennard-Jones parameters used in prior work and referred to as sets A and B. The polarizability used in the present work is consistent with the original parametrization of the nitrate anion by Salvador et al.[38]

We employed a force field for nitrate that was adapted from Salvador et al.[38] Because of a slight difference in the van der Waals parameters reported by Salvador et al.[38] and Minofar et al.,[18] simulations were performed using both parameter sets. Simulation parameters used in previous work and in the present study are given in Table 1. The polarizability of the nitrate anion originally recommended by Salvador et al., 1.49 Å^3 placed on each of the three nitrate oxygen atoms, was used in the present work. The geometry of the nitrate is maintained by the real N−O bond (1.269 Å) and an artificial O−O bond (2.197 Å) used to constrain the molecule during the simulation. The performance of the force field in reproducing the bulk properties of aqueous sodium nitrate solutions, including neutron and X-ray diffraction results, and the calculated density as a function of concentration, will be reported in a subsequent publication.[73]

The surface tension and surface potential data for $NaNO_3$ solutions were calculated using methods described in detail elsewhere.[17,74] Briefly, the surface tension is calculated using:

$$\gamma = \frac{1}{2} L_z \left\langle P_{zz} - \frac{1}{2}(P_{xx} + P_{yy}) \right\rangle \quad (1)$$

where the P_{ii} are the components of the pressure tensor (calculated in the usual way from the virial expression),[64] L_z is the length of the simulation cell in the *z* direction (normal to the slab), the angular brackets denote a time average, and the factor of $^1/_2$ accounts for the slab having two interfaces. The difference between the calculated surface tension for an aqueous $NaNO_3$ slab and a neat water slab ($\Delta\gamma = \gamma_{NaNO_3} - \gamma_{H_2O}$) is reported for each concentration. The surface potential, χ, was calculated as function of the *z* coordinate by adding the contributions of the partial charges and the induced dipole moments, which gives the total surface potential. The difference in surface potential between an aqueous sodium nitrate slab and a neat water slab ($\Delta\chi = \chi_{NaNO_3} - \chi_{H_2O}$) is compared with measured surface potential data.

The magnitude and direction of the nitrate dipole for snapshots taken from classical simulations of one nitrate in water were calculated using Gaussian 03.[75] The waters were represented as point charges with $q_H = +0.41$e and $q_O = -0.82$e.[15] Single-point MP2[76] calculations were performed using the aug-cc-pvtz[77] basis set. The sodium ion was not included in these calculations.

Results and Discussion

Comparison with Experiments. The details of each simulation box, including the number of ions and water molecules, and surface tension data for three concentrations, are reported

TABLE 2: Comparison of Calculated and Measured Surface Tension[82] and Surface Potential[31] Data for Aqueous $NaNO_3$[a]

number of molecules	slab molarity (M)	calculated $\Delta\gamma$ parameter set A (dynes/cm)	calculated $\Delta\gamma$ parameter set B (dynes/cm)	measured $\Delta\gamma$[82] (dynes/cm)	calculated $\Delta\chi$ parameter set A (mV)	calculated $\Delta\chi$ parameter set B (mV)	measured $\Delta\chi$[31] (mV)
18 $NaNO_3$ 864 H_2O	1.5	0.6 ± 1.6	-1.5 ± 1.4	1.8 ± 0.2	100	60	25
86 $NaNO_3$ 864 H_2O	6.8	8.1 ± 2.3	7.1 ± 3.2	7.3 ± 0.6	400	280	−
141 $NaNO_3$ 864 H_2O	8.5	11.6 ± 2.8	7.7 ± 3.2	8.8 ± 0.6	−	−	−

[a] Errors for surface tension data were estimated using the method of blocking transforms.[78]

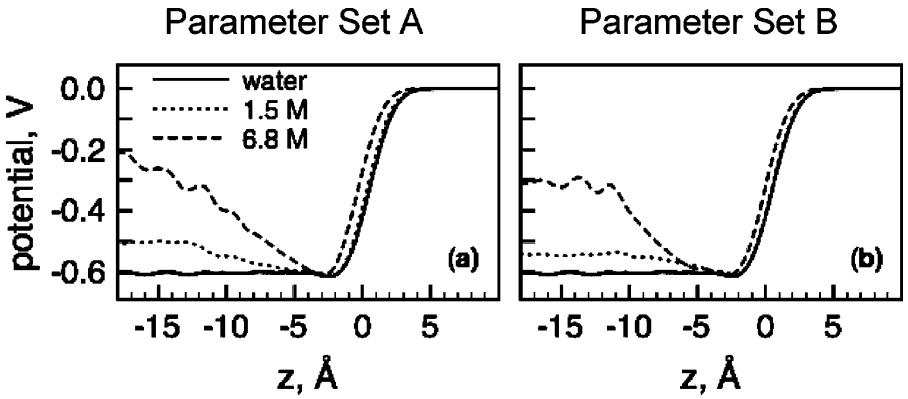

Figure 2. Surface potentials for 1.5 and 6.8 M $NaNO_3$ compared to the surface potential of water, computed using 2 ns of simulation data. Data is shown relative to the Gibbs dividing surface, set to $z = 0$. The difference in the potential for $NaNO_3$ solutions and neat water is compared to experimental data in the text.

in Table 2. The $NaNO_3$ concentration for each slab with finite concentration was determined by calculating the average molarity of the center 20 Å of the slab in the z direction. The calculated molarity of the most concentrated solution is slightly above the solubility limit (7.8 M) for $NaNO_3$. The presence of measured surface tension data for supersaturated solutions makes it relevant to calculate the surface tension for 8.5 M $NaNO_3$ and compare it against experiment. To compare the surface tension of our simulations to available surface tension data (up to 12.2 M), the experimental data was fit to a polynomial that describes a general relationship between molarity and surface tension. As the simulated solution approaches the solubility limit, the degree of ion clustering increases dramatically and small domains of $NaNO_3$ begin to form in the solution at the onset of crystallization. This ion clustering in the 8.5 M simulations limits their usefulness in providing insight into the structural properties of aqueous $NaNO_3$. The discussion of structural properties is therefore limited to simulations below the solubility limit. Calculation of the surface tension and surface potential was restricted to finite concentrations because the simulation length needed to calculate these values for the "infinite dilution" within error is longer than currently feasible.

Surface tension data ($\Delta\gamma = \gamma_{NaNO_3} - \gamma_{H_2O}$) were calculated using 1.6 ns of simulation data for water and 3.3 ns of simulation data for the $NaNO_3$ slabs. Both sets of Lennard-Jones parameters produce reasonable surface tension data, however, parameter set B is better at reproducing the surface tension of the most concentrated slab. The $\Delta\gamma$ value for 1.5 M $NaNO_3$ has the wrong sign using parameter set B, but is within 2σ of error. Error bars were calculated using blocking transformations, a method for estimating the statistical error in correlated data proposed by Flyvbjerg and Petersen[78] and described in more detail by Benz et al.[79]

The electrostatic surface potential was calculated for water and $NaNO_3$ slabs at two concentrations using both parameter sets A and B and is shown in Table 2. Figure 2 shows the potential as a function of z coordinate relative to the Gibbs dividing surface for water, 1.5 and 6.8 M $NaNO_3$. In this study, we use the approximate definition that the Gibbs dividing surface is located where the interfacial water density is half its bulk value. Subtracting the water potential in the center of the slab from the $NaNO_3$ potential gives $\Delta\chi$ values that can be compared with experimental data, which is measured as a difference from neat water. For 1.5 M $NaNO_3$, the measured $\Delta\chi$ is 0.03 V and increases with concentration.[31] Consistent with the experimental data, the calculated values are positive and increasing with concentration with both parameter sets. The absence of measured surface potential data above 2.0 molal (~3 M) limits us to comparing the surface potential trend, rather than compare with measured data for 6.8 M $NaNO_3$. For parameter set A (Figure 2a), the potentials differ from water by 0.1 V (1.5 M) and 0.4 V (6.8 M). For parameter set B (Figure 2b), the potentials differ from water by 0.06 V (1.5 M) and 0.28 V (6.8 M). Set B is closer to the experimental value for 1.5 M. In

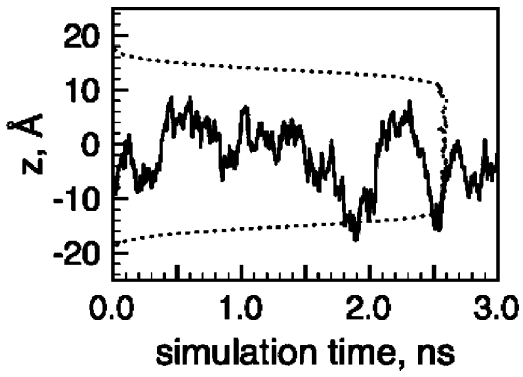

Figure 3. Nitrate z coordinate vs time (solid line) for one nitrate ion in a water slab. The water density profile (dashed line) is shown as a reference for the position of the ion in the slab.

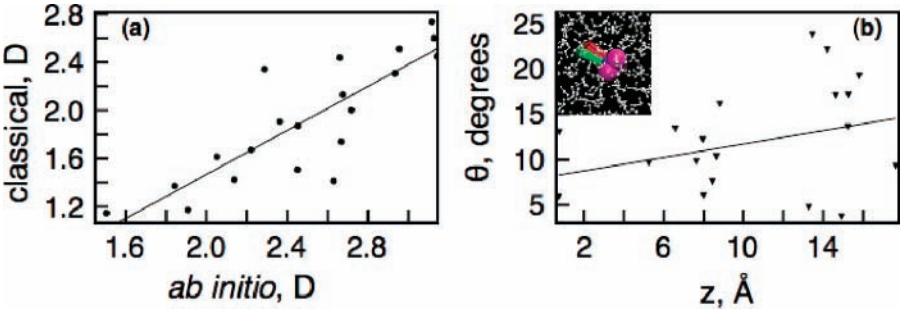

Figure 4. Magnitude of nitrate dipole, shown in (a), for one nitrate ion in a water slab from the classical Amber simulation vs the dipole calculated at the MP2/aug-cc-pVTZ level with the waters represented as point charges. The angle between the classical and ab initio dipole vs the distance from the center of the slab is shown in (b). A snapshot of the two dipoles is shown with the classical dipole in red and the ab initio dipole in green.

addition, the rate of increase with concentration is in closer agreement with experimental data for parameter set B.

Surface tension and surface potential calculations suggest that parameter set B is in slightly closer agreement with experimental data. In addition, parameter set B (modified by reducing the polarizability by 20%), has recently been shown to give a free energy of hydration in good agreement with experimental data for the nitrate anion.[18] The structural properties for both data sets are quite similar, hence in the remainder of the paper, only results for parameter set B are shown.

$NaNO_3$ at Infinite Dilution. Simulations of one $NaNO_3$ in a water slab were completed in order to compare with simulations carried out by Salvador et al.[38] in which a single nitrate anion was placed on the surface of a water slab. When a polarizable model was used, the anion remained near the surface, but when a nonpolarizable model was used, the anion spent most of the time in the interior of the slab. The prior study therefore concluded that, if polarization is taken into account, the nitrate anion has a propensity for the air−water interface.

The corresponding results from the present study are shown in Figure 3 employing a polarizable force field with nitrate placed initially in the bulk of the slab. Similar results were obtained with both parameter sets in 3 ns runs with the nitrate initially placed at the interface. All of our simulations show that nitrate resides at the interface for short times but returns to the bulk of the slab. On average, the nitrate anion spends relatively little time at the interface.

In the force field used in the present simulations, the nitrate polarization is modeled by dividing the NO_3^- polarizability into three equal contributions of 1.49 $Å^3$ placed n the oxygen atoms. To verify that this accurately represents the anisotropic nature of the nitrate polarizability, with a large difference between the in-plane and out-of-plane components,[38] single-point ab initio electronic structure calculations were performed on one nitrate ion in solution. Coordinates of one nitrate ion in 864 water molecules were taken from snapshots of classical simulations, and the water oxygen and hydrogen atoms were replaced by point charges.[15] The sodium ion was not included in the single-point calculations but is expected to have a minimal impact on the nitrate dipole because the nitrate and sodium ions were well separated in the snapshots used for these calculations. Figure 4a shows the magnitude of the instantaneous dipole moment in the force field-based simulation vs the corresponding ab initio dipole moment. The force field and ab initio dipole moments have similar magnitudes, which differ by around 30%. Figure 4b shows the angle between the ab initio and force field dipole moments in degrees for both parameter sets as a function of position within the slab. The angle between the dipoles ranges between 2° and 25°, with a slight trend toward larger differences as the ion moves toward the interface. It is clear from this analysis that distributing the polarizability equally on the three oxygen atoms in nitrate represents both the magnitude and the direction of the nitrate dipole reasonably well.

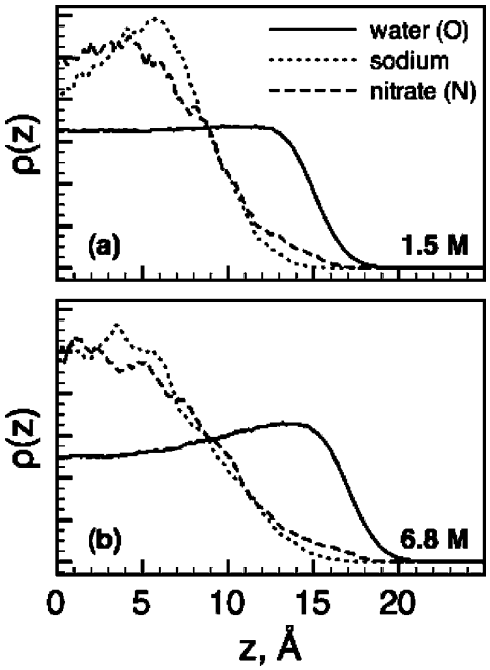

Figure 5. Density profiles for water oxygen (solid line), sodium (dotted line), and nitrate nitrogen (dashed line) for 1.5 M (a) and 6.8 M (c), respectively, shown for simulations using 4 ns of simulation data.

Interfacial Structure of Aqueous Solutions of $NaNO_3$ at Finite Concentrations. The surface propensity of the nitrate anion, represented as a density profile, is shown for 1.5 and 6.8 M sodium nitrate simulations in Figure 5. For ease of comparison, each density profile was normalized using $\int_{z_{min}}^{z_{max}} \rho(z)\, dz = 1$ and averaged about the center of the slab. In all cases, the nitrate anion resides primarily below the first few surface water layers and has only a small probability of being at the surface of the solution.

Recently a free-energy decomposition of the factors (such as cavity formation, permanent change, and polarizability) that stabilize surface solvation was presented for iodide, a spherical ion.[80] In their analysis, Archontis and Leontidis found that permanent charge interactions favor the bulk, while induced-dipole moments stabilize the interface. However, delocalization of the polarizability onto the three oxygen atoms does not appear to be the origin of bulk solvation of the nitrate ion in our simulations because, in recent simulations of aqueous KNO_3 by Dang et al., the polarizability of the nitrate ion was placed only on the central nitrogen and bulk solvation was also observed.[11] The isotropic polarizability (the mean value of the

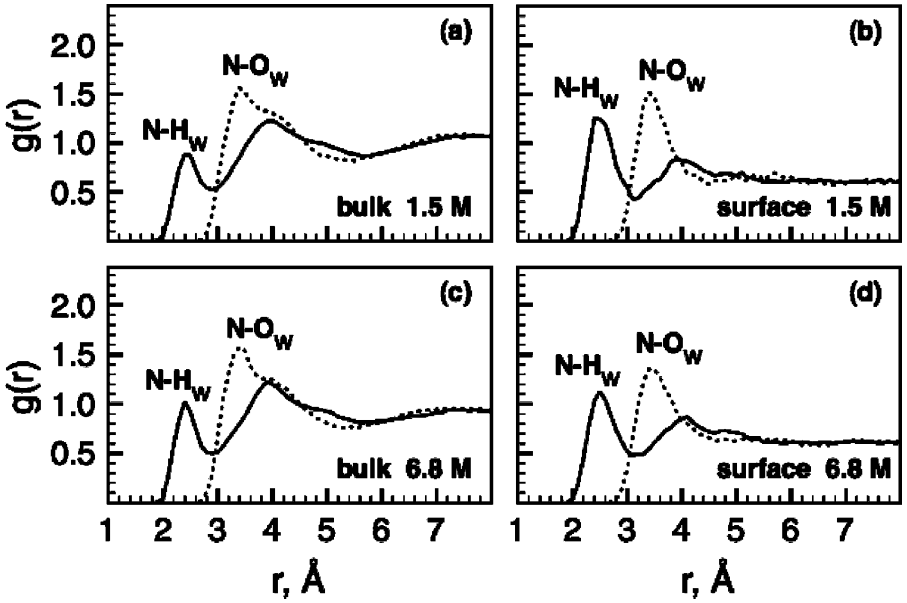

Figure 6. Nitrate−water oxygen radial distribution functions, $g(r)$, for bulk and near surface ions in 1.5 and 6.8 M $NaNO_3$ slabs.

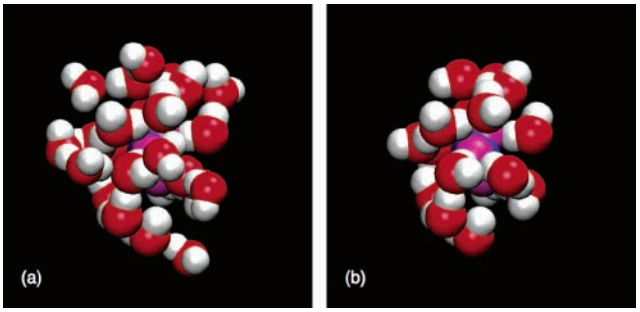

Figure 7. Snapshots of the coordination shell around one bulk NO_3^- ion in 6.8 M $NaNO_3$. The solvation shell (a) with waters shown as a shoulder in the bulk radial distribution function ($r \sim 4.5$ Å in Figure 6a) and (b) with waters less than 4.0 Å from the nitrate; these waters are closer to the nitrate than those represented as a shoulder in the RDF.

in-plane ($\alpha_{||}$) and the out-of-plane ($\alpha_{\perp}$) polarizability) of a hydrated NO_3^-, 4.47 Å^3, is almost the same as that of the bromide anion (4.53 Å^3),[81] which exhibits a clear propensity for the air−water interface. Obviously, the factors stabilizing the bulk versus interfacial solvation of molecular ions are more complex than those in the case of spherical ions due to multiple hydrogen-bonding sites and also differences in size and shape.

Nitrate solvation was investigated by calculating radial distribution functions (RDF) as a function of z coordinate in the slab. Figure 6 shows RDFs for 1.5 M $NaNO_3$ for bulk (a) and surface (b) ions and the corresponding plots for 6.8 M $NaNO_3$ in (c) and (d). For this analysis, bulk and surface ions were located within 2.5 Å and between $z = 12.5-15$ Å from the center of the slab, respectively. The N−O$_w$ RDFs for the bulk ions have a bimodal character, with a shoulder at $r \sim 4.5$ Å corresponding to a second water shell. This is illustrated in Figure 7, showing snapshots of one nitrate with its solvation shell: (a) including the shoulder (all waters within 5.0 Å) and (b) not including the shoulder (only waters within 4.0 Å). This shoulder is not apparent in the N−O$_w$ RDFs for surface ions. A decrease in the peak maximum around $r = 4$ Å in the N−H$_w$ RDF also shows a difference between bulk and surface ions. The first peak in the N−H$_w$ RDF around $r = 2.6$ Å is predominantly due to the hydrogen atoms that are hydrogen-bonded to the nitrate oxygen. This kind of "lateral" solvation will be a favorable arrangement particularly on the surface, where the nitrate ion exhibits a preferred orientation parallel to the surface (see below). This is reflected in the strong first peak in the N−H$_w$ RDF on the surface, while the second peak is much less pronounced. However, in the isotropic conditions of the bulk, both peaks are of comparable intensity. Both the N−O$_w$ and N−H$_w$ first peaks are more pronounced at the surface compared to the bulk. This suggests that surface nitrates bind waters more strongly. While at the surface, nitrate ions remain parallel to the interface (see below) in order to maximize interactions of all nitrate oxygens with water hydrogens.

In Figure 8, the total number of waters in the solvation shell around nitrate ions as a function of z coordinate is shown. The radial distribution function was calculated in 2.5 Å bins in the z direction starting with $z = 0$, the center of the slab. Then, the first minimum in each N−O$_W$ RDF was used to define the coordination number, i.e., the total number of water molecules that form a coordination cage around the nitrate ions. Defining the water coordination by the first minimum in each RDF clearly includes waters in both the first and second solvation shell for bulk ions, which are shown in the N−O$_W$ RDF as a shoulder at $r = 4.5$ Å. This is the most unambiguous definition for water coordination that avoids the difficulty of decomposing contributions from the first bimodal N−O$_w$ RDF peak and provides the information needed to identify potential differences in solvent cage effects between bulk and surface ions. For both concentrations, nitrates near the surface have fewer water molecules surrounding them than bulk ions. There is a decrease in the number of waters coordinating near surface nitrates due to the absence of waters in the vacuum region above (or below) the slab. This effect is quantified in Figure 8 and provides evidence that surface nitrates could exhibit unique chemistry due to the reduced solvent cage surrounding them.

To make contact with surface-sensitive vibrational spectroscopy experiments, the density (number per unit volume) of free OH bonds for neat water, 1.5 M $NaNO_3$ and 6.8 M $NaNO_3$, is plotted as a function of position in the slab relative to the Gibbs dividing surface in Figure 9. An OH bond is considered hydrogen-bonded if the donor H to acceptor O distance is less than the first minimum in the corresponding radial distribution function and the O$_w$−H$_w$−O$_{\text{hydrogen bond}}$ angle is less than 30°. The distance cutoff for the intermolecular hydrogen bond is 2.4 Å for H$_w$−O$_w$ and 2.2 Å for H$_w$−O$_{\text{nitrate}}$. This definition has

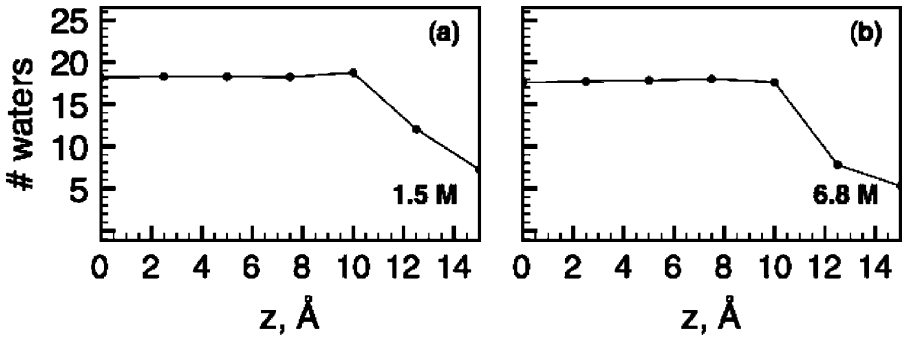

Figure 8. The total number of waters in the solvation shell (defined by the first minimum in the radial distribution function) as a function of position in the slab. In these plots, $z = 0$ is the center of the slab and $z = 15$ is near the interface.

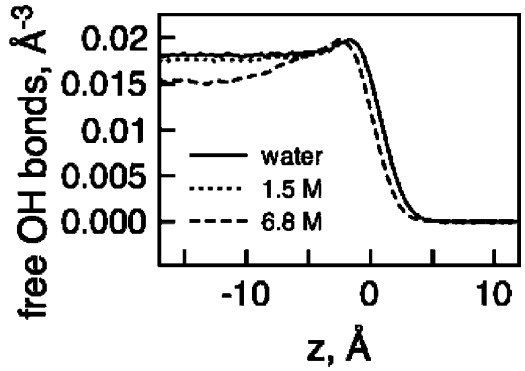

Figure 9. Population of free OH bonds (water OH bonds not involved in a hydrogen bond with either another water or nitrate oxygen) for neat water (solid line), 1.5 M $NaNO_3$ (dotted line), and 6.8 M $NaNO_3$ (dashed line), using parameter set B. Shown relative to $z = 0$, representing the Gibbs dividing surface.

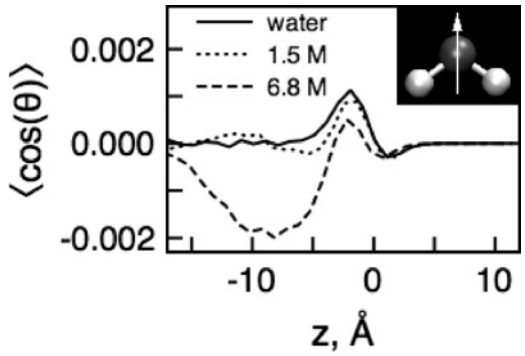

Figure 10. Water orientation as a function of position in the slab relative to the Gibbs dividing surface ($z = 0$). The water orientational order parameter for water (solid line), 1.5 M (dotted line), and 6.8 M (dashed line) $NaNO_3$.

been used by a variety of groups and is referred to as a "normal" hydrogen bond by Walker and co-workers.[29] Figure 9 shows that the total number of free OH bonds is similar for 1.5 M $NaNO_3$ and neat water, while the number of free OH bonds is less for 6.8 M $NaNO_3$.

The orientation of water molecules and nitrate ions as a function of position in the interfacial region was also investigated. The orientational order parameter for water molecules, $\langle\cos(\theta)\rangle$, where θ is the angle between the water dipole and the surface normal and the brackets denote an average over molecules and time, is plotted in Figure 10. To directly compare orientational order parameter peak positions, the data is shown relative to the Gibbs dividing surface (set to $z = 0$). Note that the order parameter is zero for an isotropic angular distribution, and nonzero values correspond to net orientational order. The orientational distribution of water molecules in the interfacial region of nitrate solutions is significantly different from neat water, but only at high concentrations and mainly in the subsurface.

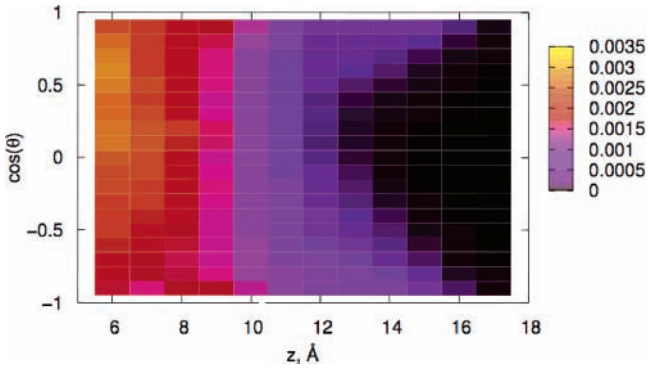

Figure 11. Nitrate orientation for 1.5 M $NaNO_3$ as a histogram of $\cos(\theta)$ values, where θ is the angle between a vector pointing out of the nitrate plane and the $\hat{z}$ unit vector. When the nitrate oxygens are in the same plane as the interface, $\cos(\theta)$ will either be 1 or -1.

Using the free OH population in combination with the water orientational order parameter, a qualitative comparison with the vibrational sum frequency generation data published by Schnitzer et al.[25] is possible. The orientational order for 6.8 M $NaNO_3$ (Figure 10) suggests the interface, defined by an absence of inversion symmetry, extends deeper into the slab for higher concentrations. A decrease in the total free OH (suggested from the free OH population), and the increase in free OH due to deepening of the interface (suggested from the orientational order parameter), would affect the VSFG signal in opposite ways. The lower OH stretch intensity at 3700 cm^{-1} for $0.2x$ $NaNO_3$ (x = mole fraction) compared to both $0.01x$ $NaNO_3$ and neat water suggests that the population of free OH oscillators decreases with $NaNO_3$ concentration. However, identification of the specific factors contributing to this decrease would require further analysis.

The nitrate orientation was investigated by defining θ as the angle between the surface normal and a vector normal to the nitrate plane. For the planar nitrate anion, $\langle\cos(\theta)\rangle$ is not a useful orientational order parameter because a value of $\langle\cos(\theta)\rangle = 0$ could indicate either that there is no preferential orientation or that all the nitrate ions are oriented with their oxygen atoms in the plane of the interface. To avoid this ambiguity, a histogram of $\cos(\theta)$ values as a function of position in the slab was calculated instead of $\langle\cos(\theta)\rangle$. The histograms computed in 1 Å bins along the surface normal are plotted in Figure 11 for 1.5 M $NaNO_3$ using parameter set B. Equal intensity in all $\cos(\theta)$ bins indicates no preferential orientation, while a build up of intensity in one region of $\cos(\theta)$, for a given z value, indicates a preferred orientation. Nitrate ions in the bulk region of the slab, $z < 8$ Å, do not have a preferred orientation. There is a

build up in the $\cos(\theta) = 1$ and -1 bins as the ions approach the interface. Note that, in absolute terms, the intensity decreases with increasing z coordinate due to a decrease in the total number of nitrate ions present in the interfacial region of the slab (see density profiles). Similar results (not shown) were obtained for the 6.8 M concentration. This indicates that interfacial nitrate ions are oriented preferentially, with their planes parallel to the interface.

Conclusions

The behavior of $NaNO_3$ at aqueous interfaces has been investigated using classical molecular dynamics simulations. The accuracy of the force fields used in the simulations has been established by comparison with experimental surface tension and surface potential data and ab initio electronic structure calculations. Nitrate was found to reside primarily below the air−water interface. Interfacial nitrate ions were found to have a preferred orientation and were solvated by fewer water molecules than bulk nitrate ions. Further experimental studies on the nitrate ion at aqueous interfaces to determine its interfacial propensity and to characterize reactivity are clearly warranted.

Acknowledgment. We thank Barbara J. Finalyson-Pitts, Benny Gerber, Ryan W. Benz, Raffaella D'Auria, Pavel Jungwirth, Martin Mucha, Luboš Vrbka, Babak Minofar, and Robert Vácha for helpful discussions. This work is supported by the Collaborative Research in Chemistry program and the AirUCI Environmental Molecular Science Institute funded by the National Science Foundation (grants CHE-0209719 and CHE-0431312). J.T. thanks the Department of Energy and the National Science Foundation for supporting the Interfacial and Condensed Phase Chemical Physics Summer Research Institute at Pacific Northwest National Lab and the ARCS Foundation Inc. for a fellowship. The work at Pacific Northwest National Laboratory was performed under the auspices of the Division of Chemical Sciences, Office of Basic Energy Sciences, U.S. Department of Energy. Pacific Northwest National Laboratory is operated by Battelle for the Department of Energy. M.R. gratefully acknowledges support from the Ministry of Education of the Czech Republic (grants 1P05ME798 and LC512). Grant 1P05ME798 also supported the visit of J.T. to Prague. The work in Prague was performed within the framework of the research project Z40550506.

References and Notes

(1) Hu, J. H.; Shi, Q.; Davidovits, P.; Worsnop, D. R.; Zahniser, M. S.; Kolb, C. E. *J. Phys. Chem.* **1995**, *99*, 8768.
(2) Perera, L.; Berkowitz, M. L. *J. Chem. Phys.* **1991**, *95*, 1954.
(3) Perera, L.; Berkowitz, M. L. *J. Chem. Phys.* **1993**, *99*, 4222.
(4) Knipping, E. M.; Lakin, M. J.; Foster, K. L.; Jungwirth, P.; Tobias, D. J.; Gerber, R. B.; Dabdub, D.; Finlayson-Pitts, B. J. *Science* **2000**, *288*, 301.
(5) Hunt, S. W.; Roeselová, M.; Wang, W.; Wingen, L. M.; Knipping, E. M.; Tobias, D. J.; Dabdub, D.; Finlayson-Pitts, B. J. *J. Phys. Chem. A* **2004**, *108*, 11559.
(6) Gaspar, D. J.; Laskin, A.; Wang, W.; Hunt, S. W.; Finlayson-Pitts, B. J. *Appl. Surf. Sci.* **2004**, *231*, 520.
(7) Laskin, A.; Wang, H.; Robertson, W. H.; Cowin, J. P.; Ezell, M. J.; Finlayson-Pitts, B. J. *J. Phys. Chem. A* **2006**, *110*, 10619.
(8) Dang, L. X. *J. Phys. Chem. B* **2002**, *106*, 10388.
(9) Dang, L. X.; Chang, T. M. *J. Phys. Chem. B* **2002**, *106*, 235.
(10) Jungwirth, P.; Curtis, J. E.; Tobias, D. J. *Chem. Phys. Lett.* **2003**, *367*, 704.
(11) Dang, L. X.; Chang, T. M.; Roeselová, M.; Garrett, B. C.; Tobias, D. J. *J. Chem. Phys.* **2006**, *124*.
(12) Jungwirth, P.; Tobias, D. J. *J. Phys. Chem. B* **2000**, *104*, 7702.
(13) Jungwirth, P.; Tobias, D. J. *J. Phys. Chem. B* **2001**, *105*, 10468.
(14) Jungwirth, P.; Tobias, D. J. *J. Phys. Chem. B* **2002**, *106*, 6361.
(15) Jungwirth, P.; Tobias, D. J. *J. Phys. Chem. A* **2002**, *106*, 379.
(16) Jungwirth, P.; Finlayson-Pitts, B. J.; Tobias, D. J. *Chem. Rev.* **2006**, *106*, 1137.
(17) Jungwirth, P.; Tobias, D. J. *Chem. Rev.* **2006**, *106*, 1259.
(18) Minofar, B.; Vacha, R.; Wahab, A.; Mahiuddin, S.; Kunz, W.; Jungwirth, P. *J. Phys. Chem. B* **2006**, *110*, 15939.
(19) Petersen, P. B.; Johnson, J. C.; Knutsen, K. P.; Saykally, R. J. *Chem. Phys. Lett.* **2004**, *397*, 46.
(20) Petersen, P. B.; Saykally, R. J. *Chem. Phys. Lett.* **2004**, *397*, 51.
(21) Petersen, P. B.; Saykally, R. J.; Mucha, M.; Jungwirth, P. *J. Phys. Chem. B* **2005**, *109*, 10915.
(22) Petersen, P. B.; Saykally, R. J. *J. Am. Chem. Soc.* **2005**, *127*, 15446.
(23) Petersen, P. B.; Saykally, R. J. *Annu. Rev. Phys. Chem.* **2006**, *57*, 333.
(24) Petersen, P. B.; Saykally, R. J. *J. Phys. Chem. B* **2006**, *110*, 14060.
(25) Schnitzer, C.; Baldelli, S.; Shultz, M. J. *J. Phys. Chem. B* **2000**, *104*, 585.
(26) Raymond, E. A.; Richmond, G. L. *J. Phys. Chem. B* **2004**, *108*, 5051.
(27) Mucha, M.; Frigato, T.; Levering, L. M.; Allen, H. C.; Tobias, D. J.; Dang, L. X.; Jungwirth, P. *J. Phys. Chem. B* **2005**, *109*, 7617.
(28) Brown, E. C.; Mucha, M.; Jungwirth, P.; Tobias, D. J. *J. Phys. Chem. B* **2005**, *109*, 7934.
(29) Walker, D. S.; Hore, D. K.; Richmond, G. L. *J. Phys. Chem. B* **2006**, *110*, 20451.
(30) Onsager, L.; Samaras, N. N. S. *J. Chem. Phys.* **1934**, *2*, 528.
(31) Randles, J. E. B. *Phys. Chem. Liq.* **1977**, *7*, 107.
(32) Pegram, L. M.; Record, J. M. T. *Proc. Natl. Acad. Sci. U.S.A.* **2006**, *103*, 14278.
(33) Honrath, R. E.; Peterson, M. C.; Guo, S.; Dibb, J. E.; Shepson, P. B.; Campbell, B. *Geophys. Res. Lett.* **1999**, *26*, 695.
(34) Dubowski, Y.; Colussi, A. J.; Hoffmann, M. R. *J. Phys. Chem. A* **2001**, *105*, 4928.
(35) Simpson, W. R.; King, M. D.; Beine, H. J.; Honrath, R. E.; Zhou, X. L. *Atmos. Environ.* **2002**, *36*, 2663.
(36) Domine, F.; Shepson, P. B. *Science* **2002**, *297*, 1506.
(37) Dubowski, Y.; Colussi, A. J.; Boxe, C.; Hoffmann, M. R. *J. Phys. Chem. A* **2002**, *106*, 6967.
(38) Salvador, P.; Curtis, J. E.; Tobias, D. J.; Jungwirth, P. *Phys. Chem. Chem. Phys.* **2003**, *5*, 3752.
(39) Boxe, C. S.; Colussi, A. J.; Hoffmann, M. R.; Tan, D.; Mastromarino, J.; Case, A. T.; Sandholm, S. T.; Davis, D. D. *J. Phys. Chem. A* **2003**, *107*, 11409.
(40) Zhang, Q.; Anastasio, C. *Environ. Sci. Technol.* **2003**, *37*, 3522.
(41) Chu, L.; Anastasio, C. *J. Phys. Chem. A* **2003**, *107*, 9594.
(42) Hoffman, R. C.; Laskin, A.; Finlayson-Pitts, B. J. *J. Aerosol Sci.* **2004**, *35*, 869.
(43) Dassau, T. M.; Shepson, P. B.; Bottenheim, J. W.; Ford, K. M. *J. Geophys. Res.* **2004**, *109*, D18302.
(44) Dubowski, Y.; Sumner, A. L.; Menke, E. J.; Gaspar, D. J.; Newberg, J. T.; Hoffman, R. C.; Penner, R. M.; Hemminger, J. C.; Finlayson-Pitts, B. J. *Phys. Chem. Chem. Phys.* **2004**, *6*, 3879.
(45) Boxe, C. S.; Colussi, A. J.; Hoffmann, M. R.; Murphy, J. G.; Wooldridge, P. J.; Bertram, T. H.; Cohen, R. C. *J. Phys. Chem. A* **2005**, *109*, 8520.
(46) Morino, Y.; Kondo, Y.; Takegawa, N.; Miyazaki, Y.; Kita, K.; Komazaki, Y.; Fukuda, M.; Miyakawa, T.; Moteki, N.; Worsnop, D. R. *J. Geophys. Res.* **2006**, *111*, D15215.
(47) Chow, J. C.; Chen, L. W. A.; Watson, J. G.; Lowenthal, D. H.; Magliano, K. A.; Turkiewicz, K.; Lehrman, D. E. *J. Geophys. Res.* **2006**, *111*, D10S04.
(48) Gibson, E. R.; Hudson, P. K.; Grassian, V. H. *J. Phys. Chem. A* **2006**, *110*, 11785.
(49) Boxe, C. S.; Colussi, A. J.; Hoffmann, M. R.; Perez, I. M.; Murphy, J. G.; Cohen, R. C. *J. Phys. Chem. A* **2006**, *110*, 3578.
(50) Finlayson-Pitts, B. J.; Hemminger, J. C. *J. Phys. Chem. A* **2000**, *104*, 11463.
(51) Laskin, A.; Iedema, M. J.; Cowin, J. P. *Environ. Sci. Technol.* **2002**, *36*, 4948.
(52) Rossi, M. J. *Chem. Rev.* **2003**, *103*, 4823.
(53) Finlayson-Pitts, B. J. *Chem. Rev.* **2003**, *103*, 4801.
(54) Dall'Osto, M.; Beddows, D. C. S.; Kinnersley, R. P.; Harrison, R. M.; Donovan, R. J.; Heal, M. R. *J. Geophys. Res.* **2004**, *109*, D21302.
(55) Niemi, J. V.; Saarikoski, S.; Tervahattu, H.; Makela, T.; Hillamo, R.; Vehkamaki, H.; Sogacheva, L.; Kulmala, M. *Atmos. Chem. Phys.* **2006**, *6*, 5049.
(56) Laskin, A.; Cowin, J. P.; Iedema, M. J. *J. Electron. Spectrosc. Relat. Phenom.* **2006**, *150*, 260.
(57) Finlayson-Pitts, B. J.; Pitts, J. M. J. *Chemistry of the Upper and Lower Atmosphere*; Academic Press: San Diego, 2000.
(58) Morita, A.; Hynes, J. T. *Chem. Phys.* **2000**, *258*, 371.
(59) Morita, A.; Hynes, J. T. *J. Phys. Chem. B* **2002**, *106*, 673.
(60) Perry, A.; Ahlborn, H.; Space, B.; Moore, P. B. *J. Chem. Phys.* **2003**, *118*, 8411.

(61) Perry, A.; Neipert, C.; Kasprzyk, C. R.; Green, T.; Space, B.; Moore, P. B. *J. Chem. Phys.* **2005**, *123*, 144705.
(62) Perry, A.; Neipert, C.; Ridley, C.; Space, B.; Moore, P. B. *Phys. Rev. E* **2005**, *71*, 050601(R).
(63) Perry, A.; Neipert, C.; Space, B.; Moore, P. B. *Chem. Rev.* **2006**, *106*, 1234.
(64) Allen, M. P.; Tildesley, D. J. *Computer Simulation of Liquids*; Clarendon: Oxford, 1987.
(65) Benjamin, I. *J. Chem. Phys.* **1991**, *95*, 3698.
(66) Wilson, M. A.; Pohorille, A. *J. Chem. Phys.* **1991**, *95*, 6005.
(67) Case, D. A.; Darden, T. A.; Cheatham, T. E., III; Simmerling, C. L.; Wang, J.; Duke, R. E.; Luo, R.; Merz, K. M.; Wang, B.; Pearlman, D. A.; Crowley, M.; Brozell, S.; Tsui, V.; Gohlke, H.; Mongan, J.; Hornak, V.; Cui, G.; Beroza, P.; Schafmeister, C.; Caldwell, J. W.; Ross, W. S.; Kollman, P. A. *AMBER 8*; University of California: San Francisco, 2004.
(68) Darden, T.; York, D.; Pedersen, L. *J. Chem. Phys.* **1993**, *98*, 10089.
(69) Essmann, U.; Perera, L.; Berkowitz, M. L.; Darden, T.; Lee, H.; Pedersen, L. G. *J. Chem. Phys.* **1995**, *103*, 8577.
(70) Caldwell, J. W.; Kollman, P. A. *J. Phys. Chem.* **1995**, *99*, 6208.
(71) Ryckaert, J. P.; Ciccotti, G.; Berendsen, H. J. C. *J. Comp. Phys.* **1977**, *23*, 327.
(72) Thole, B. T. *Chem. Phys.* **1981**, *59*, 341.
(73) Thomas, J. L.; Tobias, D. J. **2007**, in preparation.
(74) Wick, C. D.; Dang, L. X.; Jungwirth, P. *J. Chem. Phys.* **2006**, *125*, 024706.
(75) Frisch, M. J.; Trucks, G. W.; Schlegel, H. B.; Scuseria, G. E.; Robb, M. A.; Cheeseman, J. R.; Montgomery, J. A., Jr.; Vreven, T.; Kudin, K. N.; Burant, J. C.; Millam, J. M.; Iyengar, S. S.; Tomasi, J.; Barone, V.; Mennucci, B.; Cossi, M.; Scalmani, G.; Rega, N.; Petersson, G. A.; Nakatsuji, H.; Hada, M.; Ehara, M.; Toyota, K.; Fukuda, R.; Hasegawa, J.; Ishida, M.; Nakajima, T.; Honda, Y.; Kitao, O.; Nakai, H.; Klene, M.; Li, X.; Knox, J. E.; Hratchian, H. P.; Cross, J. B.; Bakken, V.; Adamo, C.; Jaramillo, J.; Gomperts, R.; Stratmann, R. E.; Yazyev, O.; Austin, A. J.; Cammi, R.; Pomelli, C.; Ochterski, J. W.; Ayala, P. Y.; Morokuma, K.; Voth, G. A.; Salvador, P.; Dannenberg, J. J.; Zakrzewski, V. G.; Dapprich, S.; Daniels, A. D.; Strain, M. C.; Farkas, O.; Malick, D. K.; Rabuck, A. D.; Raghavachari, K.; Foresman, J. B.; Ortiz, J. V.; Cui, Q.; Baboul, A. G.; Clifford, S.; Cioslowski, J.; Stefanov, B. B.; Liu, G.; Liashenko, A.; Piskorz, P.; Komaromi, I.; Martin, R. L.; Fox, D. J.; Keith, T.; Al-Laham, M. A.; Peng, C. Y.; Nanayakkara, A.; Challacombe, M.; Gill, P. M. W.; Johnson, B.; Chen, W.; Wong, M. W.; Gonzalez, C.; Pople, J. A. *Gaussian 03*, revision C.02; Gaussian, Inc.: Wallingford, CT, 2004.
(76) Møller, C.; Plesset, M. S. *Phys. Rev.* **1934**, *46*, 618.
(77) Kendall, R. A.; Dunning, T. H.; Harrison, R. J. *J. Chem. Phys.* **1992**, *96*, 6796.
(78) Flyvbjerg, H.; Petersen, H. G. *J. Chem. Phys.* **1989**, *91*, 461.
(79) Benz, R. W.; Castro-Roman, F.; Tobias, D. J.; White, S. H. *Biophys. J.* **2005**, *88*, 805.
(80) Archontis, G.; Leontidis, E. *Chem. Phys. Lett.* **2006**, *420*, 199.
(81) Sremaniak, L. S.; Perera, L.; Berkowitz, M. L. *Chem. Phys. Lett.* **1994**, *218*, 377.
(82) Washburn, E. W. *International Critical Tables of Numerical Data, Physics, Chemistry and Technology*, 1st electronic ed.; Knovel: Norwich, NY, 1926−1930, 2003.